Influence of piezoelectric hysteresis on the rotor speed characteristics in an ultrasonic motor

Jan Awrejcewicz and Larisa Dzyubak

Abstract: In this work a hysteretic dissipation in the ultrasonic motor is simulated by means of additional state variables (internal variables). The hysteretic model constructed has Masing-Bouc-Wen structure. It was demonstrated that hysteresis can lead to change for the worse of rotor speed characteristics.

1. Introduction

Piezoelectric materials due to their high efficiency are widely used in many branches of engineering as the radio engineering for stabilization of radio frequencies, the ultrasonics (underwater signalling), resonators in generators and stabilizers, ultrasonic holography, ultrasonic flaw detection, echosondes, sonars etc. Ultrasonic motors (USM) are applied in robotics, in production of autofocus-cameras etc.

In many cases linear models of piezoelectric structures do not describe some processes properly. Large deflection effects are described by mechanical nonlinearities, nonlinear strain-stress characteristics are related to material nonlinearities. Hysteretic nonlinearities are peculiar to piezoelectric materials. It should be pointed, that presence of hysteretic behaviour in piezoelectric devices is related to their "bad" characteristics. Due to hysteresis the piezoelectric samples polarization values are different at the same electric field intensity. It depends on the preliminary sample polarization. Periodic polarization changes lead to energy dissipation which is spent to heating of piezoelectric elements. In [1] Prandtl-Ishlinskii model is used to model the hysteretic nonlinearities in a piezoelectric-actuated system to avoid undesirable oscillations or instability. The constructed model was associated with experimental results. In [2] a measured hysteresis, a fit to Maxwell Slip hysteretic model and also work loops for various applied static loads are presented in the displacement vs field plane for high energy density piezoelectric actuators. The specific of the loops presented is absence of saturation, however, a slight inverse effect is observed.

Publications about USM [3] mainly point to two sources of nonlinearities: nonlinear stator-rotor contact interactions and relationship between piezo and stator. In this work the USM hysteretic

characteristics are simulated by means of additional state variables (internal variables). The hysteretic models with internal variables have Masing-Bouc-Wen structure. It was demonstrated [4] that this modelling mechanism for energy dissipation was sufficiently accurate to model loops of various shapes in accordance with a real experiment, reflecting the behavior of hysteretic systems from very different fields.

2. Description of the USM model with hysteresis

Piezoelectric actuators are the systems composed of the ultrasonic motors, power electronics and the closed loop control [3]. The ultrasonic motor scheme is shown in figure 1. It produces a rotation by utilizing the high-frequency vibrations of the stator which are transferred to the steady motion of the rotor in a frictional contact with the stator. The motor model consists of two flat cylinders, one representing the rotor, and the other the stator. Both are modelled as rigid bodies. The rotor is axially elastically supported with a rotational spring-damper element about the rotational axis of the rotor to allow the motion about this axis. The cylindrical stator is excited by means of a multilayered piezoceramic actuator generating a rotating torque vector orthogonal to the geometrical axis of the stator.

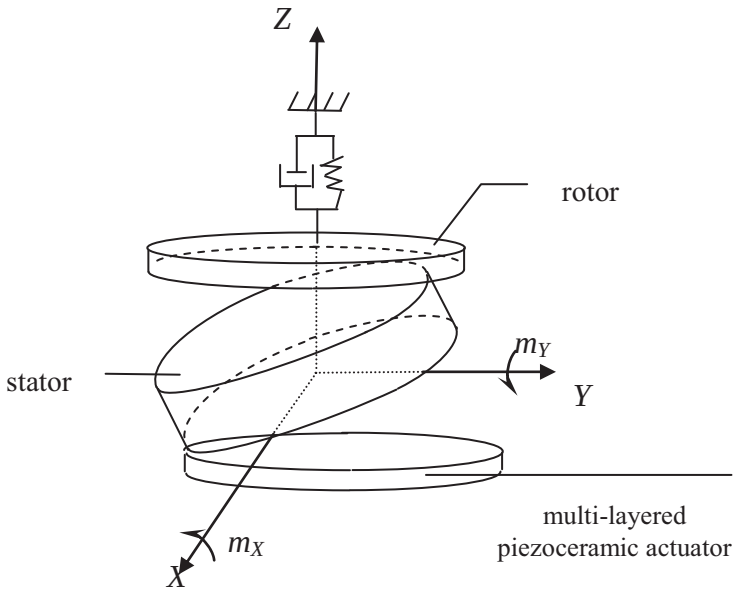

Figure1. Rigid body model of the ultrasonic motor.

One torque is generated by a sinusoidal high frequency signal, while the other follows from a cosine signal. Both signals are standing waves and mutually orthogonal. The resulting steady state vibration of the stator yields a wobbling motion of the stator disk.

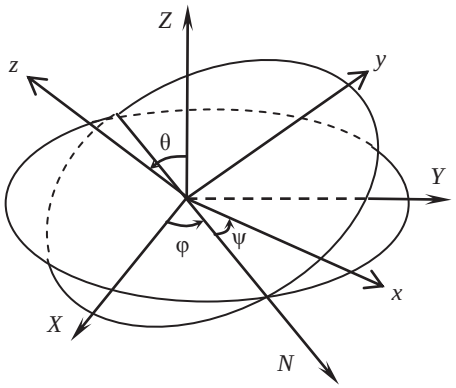

Figure 2. Euler's angles.

The governing equations of the USM with hysteretic dissipation are

$$\dot{\varphi} = \frac{\omega_x \sin\psi + \omega_y \cos\psi}{\sin\theta}, \tag{1}$$

$$\dot{\theta} = \omega_x \cos\psi - \omega_y \sin\psi, \tag{2}$$

$$\dot{\psi} = -\frac{\cos\theta\left(\omega_x \sin\psi + \omega_y \cos\psi\right)}{\sin\theta} + \omega_z, \tag{3}$$

$$I_{xx}\dot{\omega}_x = \left(I_{yy} - I_{zz}\right)\omega_y\omega_z + M_{E_x} + M_{C_x} - M_{D_x} - M_{R_x}, \tag{4}$$

$$I_{yy}\dot{\omega}_y = \left(I_{zz} - I_{xx}\right)\omega_z\omega_x + M_{E_y} + M_{C_y} - M_{D_y} - M_{R_y}, \tag{5}$$

$$I_{zz}\dot{\omega}_z = \left(I_{xx} - I_{yy}\right)\omega_x\omega_y + M_{E_z} + M_{C_z} - M_{D_z} - M_{R_z}, \tag{6}$$

$$\dot{\varphi}_R = \omega_R, \tag{7}$$

$$I_R\dot{\omega}_R = f_c R^* - T_{load}, \tag{8}$$

$$m_R\ddot{z}_R + \dot{z}_R + c_R z_R - \delta h = f_c R^* - T_{load}, \tag{9}$$

$$\begin{aligned} h(t) &= k_0(x)x(t) + \sum_{i=1}^{N} y_i(t), \\ \dot{y}_i &= \left(A_i(x) - \left(\beta_i + \alpha_i\, sgn(\dot{z})\, sgn(y_i)\right)\left|\frac{y_i}{F_i(x)}\right|^m \right)\dot{z}, \end{aligned} \tag{10}$$

The state vector is $\vec{q}(\varphi,\theta,\psi,\omega_x,\omega_y,\omega_z,\varphi_R,\omega_R,z)$. Euler's dynamical and kinematical equations (1)-(6) are equations of motion of the stator. They are formulated in the body fixed coordinate system O*xyz* (figure 2). O*XYZ* is the inertial coordinate system. O$x_1y_1z_1$ and O$x_2y_2z_2$ are two intermediate coordinate systems. The first O$x_1y_1z_1$ intermediate coordinate system is obtained from the inertial system O*XYZ* after rotation in the positive direction by an angle φ about *Oz* axis. Axis Ox_1 coincides with nodal line *N*, axis Oz_1 coincides with Oz . The second intermediate coordinate system O$x_2y_2z_2$ is obtained from the first coordinate system O$x_1y_1z_1$ after rotation in the positive direction by an angle θ about Ox_1 axis. Axis Ox_1 coincides with Ox_2, axis Oz_1 coincides with Oz_2 . Coordinate system O*xyz* is obtained from the second coordinate system O$x_2y_2z_2$ after rotation in the positive direction by an angle ψ about Oz axis.

The torque vector acting upon the stator is

$$\mathbf{M}_0 = \mathbf{M}_E + \mathbf{r}_c \times \mathbf{F}_{contact} - \mathbf{M}_R - \mathbf{M}_D \,. \tag{11}$$

$f_n, f_r, f_c,$ are normal, radial, circumferential components of the force vector $\mathbf{F}_{contact}$:

$$\mathbf{F}_{contact} = -f_n\,\mathbf{e}_Z - f_r\,\mathbf{e}_{y_1} - f_c\,\mathbf{e}_{x_1} \,. \tag{12}$$

$\mathbf{M}_E$, $\mathbf{M}_R$, $\mathbf{M}_D$ are the excitation torque generated by piezoceramic (the piezoelectric excitation is described by two given excitation torques), the restoring torque, the damping torque correspondingly:

$$\mathbf{M}_E = m_X\,\mathbf{e}_X + m_Y\,\mathbf{e}_Y \text{ with } m_X = m_0\cos\Omega t\,,\ \ m_Y = m_0\sin\Omega t\,, \tag{13}$$

$$\mathbf{M}_R = c_r\theta\,\mathbf{e}_{x_1} + c_t(\varphi+\psi\cos\theta)\mathbf{e}_Z\,, \tag{14}$$

$$\mathbf{M}_D = d_r\omega_X\,\mathbf{e}_X + d_r\omega_Y\,\mathbf{e}_Y + d_t\omega_Z\,\mathbf{e}_Z\,. \tag{15}$$

In the body-fixed coordinate system *Oxyz* torques $\mathbf{M}_E$, $\mathbf{M}_R$, $\mathbf{M}_D$, $\mathbf{M}_C$ ($\mathbf{M}_{contact}$) are expressed as

$$\begin{pmatrix} M_{E_x} \\ M_{E_y} \\ M_{E_z} \end{pmatrix} = \mathbf{A}\begin{pmatrix} m_0\cos\Omega t \\ m_0\sin\Omega t \\ 0 \end{pmatrix},\ \begin{pmatrix} M_{R_x} \\ M_{R_y} \\ M_{R_z} \end{pmatrix} = \begin{pmatrix} c_r\theta\cos\psi + c_t(\varphi+\psi\cos\theta)\sin\theta\sin\psi \\ -c_r\theta\sin\psi + c_t(\varphi+\psi\cos\theta)\sin\theta\cos\psi \\ c_t(\varphi+\psi\cos\theta)\cos\theta \end{pmatrix}, \tag{16}$$

$$\begin{pmatrix} M_{D_x} \\ M_{D_y} \\ M_{D_z} \end{pmatrix} = \mathbf{A}\begin{pmatrix} d_r\omega_X \\ d_r\omega_Y \\ d_t\omega_Z \end{pmatrix},\ \begin{pmatrix} M_{C_x} \\ M_{C_y} \\ M_{C_z} \end{pmatrix} = \mathbf{A}\begin{pmatrix} r_{C_Z}(f_c\sin\varphi + f_r\cos\varphi) - r_{C_Y}f_n \\ r_{C_X}f_n + r_{C_Z}(f_r\sin\varphi - f_c\cos\varphi) \\ r_{C_Y}(f_c\cos\varphi - f_r\sin\varphi) - r_{C_X}(f_c\sin\varphi + f_r\cos\varphi) \end{pmatrix}. \tag{17}$$

Here $\mathbf{A}$ is the transformation matrix from the inertial coordinate system with basis $\mathbf{e}_X, \mathbf{e}_Y, \mathbf{e}_Z$ to the body-fixed coordinate system with basis $\mathbf{e}_x, \mathbf{e}_y, \mathbf{e}_z$:

$$\mathbf{A}=\begin{pmatrix} cos\varphi cos\psi - sin\varphi cos\theta sin\psi & sin\varphi cos\psi + cos\varphi cos\theta sin\psi & sin\theta sin\psi \\ -cos\varphi sin\psi - sin\varphi cos\theta cos\psi & -sin\varphi sin\psi + cos\varphi cos\theta cos\psi & sin\theta cos\psi \\ sin\varphi sin\theta & -cos\varphi sin\theta & cos\theta \end{pmatrix},$$

$\mathbf{r}_c = \left(r_{C_X}, r_{C_Y}, r_{C_Z}\right)$ is the radius-vector of contact point C:

$$\mathbf{r}_c = -\left(R cos\theta - H sin\theta\right) sin\varphi\, \mathbf{e}_X + \left(R cos\theta - H sin\theta\right) cos\varphi\, \mathbf{e}_Y + \left(R sin\theta + H cos\theta\right)\mathbf{e}_Z .$$

Equations of motion of the stator (1)-(6) and rotor (7)-(9) are coupled through the dynamics at this point. The rotor disc is specified by two coordinates: rotational angle φ_R and translational coordinate z_R . Equations (7)-(8) describe the rotational motion of the rotor as well as equation (9) describes the rotor motion in the axial direction.

In hysteresis simulation a system is frequently viewed as a black box and the system's *output* (or response) is modelled with the use of analytical expressions or differential equations supposing that the *input* of the system is known. It is suggested to apply methodology that described in [4] where hysteresis is simulated by means of additional state variables:

$$z = p\left(x, y_1, y_2, ..., y_N\right), \tag{18}$$

$$\dot{y} = q\left(x, \dot{x}, y_n\right), \quad n=1, 2, \ldots, N. \tag{19}$$

Here x is an input (input signal) and z is an output (response) of the hysteretic system, p and q are nonlinear functions of its arguments, y_i (i=1, 2,…, N) are internal variables. Functions p and q are chosen depending on a loop form. The parameters of these functions are determined via a procedure minimizing the criterion function

$$\Phi\left(c_1, ...c_j, \alpha_1, ...\alpha_k, ..., \beta_1, ..., \beta_l\right) = \sum_i \left(p\left(x\left(c_1, ...c_j, t_i\right), y_1\left(\alpha_1, ...\alpha_k, t_i\right), ..., y_N\left(\beta_1, ..., \beta_l, t_i\right)\right) - z_i\right)^2 \tag{20}$$

which characterizes an error between the experimental curve and the calculated one. To this effect the gradient fall method is used.

The polarization axis and direction of the electric field of the piezoceramic in the USM is Z. Equations (10) simulate the hysteretic dissipation in the USM ($k_0(x)$, $A_i(x)\geq 0$, $F_i(x)>0$, the input signal belongs to the admissible codomain $x\in[x_{min}, x_{max}]$, $\alpha_i, \beta_i \in \mathcal{H}$). They are chosen for the USM in the form

$$\begin{aligned} h(t) &= y_1(t), \\ \dot{y}_1 &= \left(c_1 - \left(c_2 + c_3\, sgn(\dot{z})\, sgn(y_1)\right)|y_1|\right)\dot{z} \end{aligned} \tag{21}$$

Values of the parameters of equations (21) are $c_1 = 0.1$; $c_1 = 3.5$; $c_1 = 0.01$; m= 1.

3. Numerical results

Results of integrating of equations (1)-(10) are presented in figures 3-10. Figure 3 presents the hysteretic loop that reflects the hysteretic dissipation in the USM. In figures 4-5 the time history of Euler's angles φ, θ, ψ are depicted. Figures 6-8 present the components of angular velocities of the stator. In figure 9 the time history of the rotor angle φ_R is shown. Figure 10 presents the time history of the angular velocity of the rotor ω_R obtained in the frames of the model with hysteresis and without hysteresis.

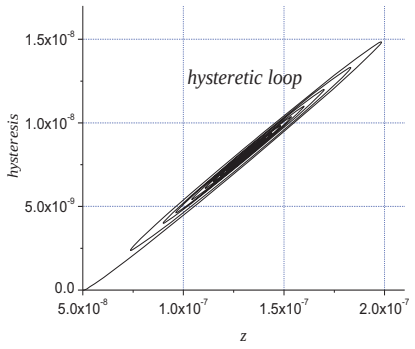

Figure 3. Hysteretic dissipation in the USM.

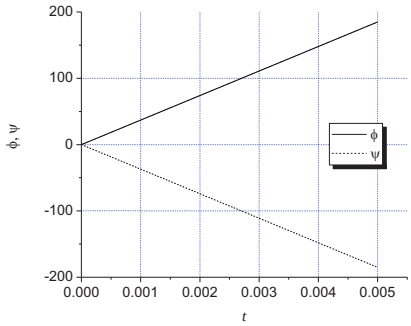

Figure 4. Time history of Euler's angles φ and ψ.

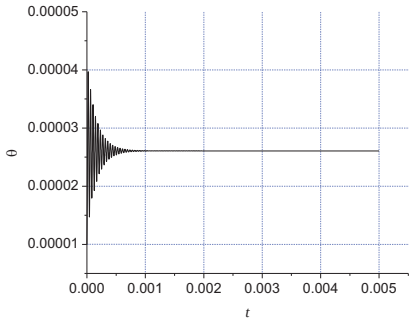

Figure 5. Time history of Euler's angle θ (the nutation angle).

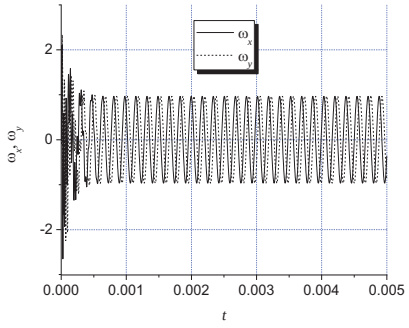

Figure 6. Time history of angular velocity components ω_x, ω_y .

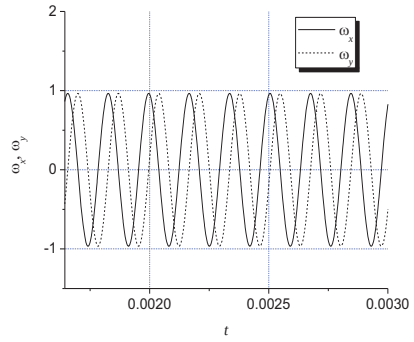

Figure 7. Time history of angular velocity components ω_x, ω_y in scale up.

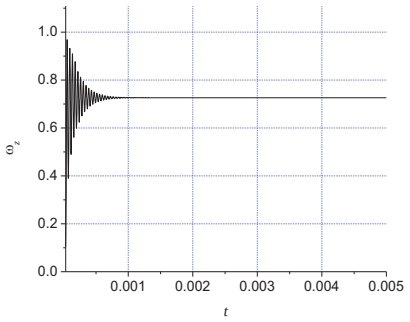

Figure 8. Time history of angular velocity component ω_z .

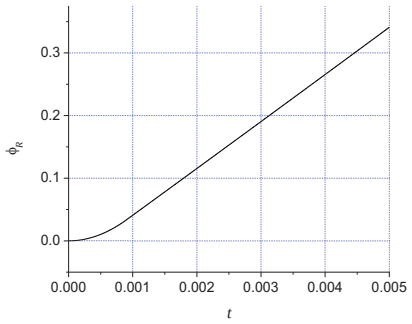

Figure 9. Time history of rotor angle φ_R .

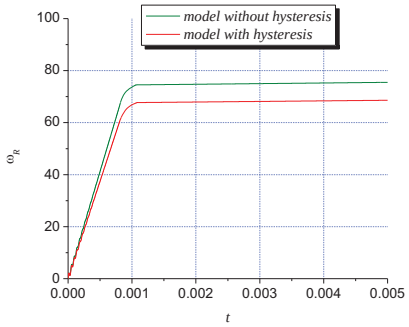

Figure 10. Time history of rotor angular velocity ω_R .

Values of accepted parameters

model parameter	value	unit
rotor disc radius	R=0.005	m
rotor disc height	H=0.003	m
rotor mass	m_R =6.4·10^{-4}	kg
rotor moment of inertia	I_R =8·10^{-9}	kgm^2
stator moment of inertia: body-fixed *x*-axis	I_{xx}=1.3·10^{-8}	kgm^2
stator moment of inertia: body-fixed *y*-axis	I_{yy}=1.3·10^{-8}	kgm^2
stator moment of inertia: body-fixed *z*-axis	I_{zz}=2.3·10^{-8}	kgm^2
Damping coefficient: axial	d_R =0.16	Ns/m
Damping coefficient: rotational (*Z*-axis)	d_t =9.1·10^{-4}	Nms/rad
damping coefficient: rotational (*X*,*Y*-axes)	d_r =1.8·10^{-4}	Nms/rad
stiffness coefficient: axial spring	c_R =4000	N/m
rotational stiffness coefficient (*Z*-axis)	c_t =10000	Nm/rad
rotational stiffness coefficient (*X*,*Y*-axes)	c_r =700	Nm/rad
external loading torque	T_{load}=0.0006	Nmm
precompression force	f_0=0.4	N
Amplitude of high frequency excitation signal	m_0 =0.02	Nm
high frequency excitation signal	Ω=37000	Hz

4. Conclusions

It was shown that at definite parameters a hysteretic dissipation in the USM can decrease the rotor speed as well as expand the rotor transition to a steady state motion. The constructed model with additional state variables (internal variables), that has Masing-Bouc-Wen structure, is appropriate to simulate hysteresis in USM. Taking into account of hysteretic dissipation based on parameter identification with a real experimental data can be useful for development and optimization of motor design and electronic drive circuit units.

The next step of the study could be an analysis of possible influence of hysteretic dissipation and a transient chaotic behaviour on the USM characteristics in various control parameter planes. The effective algorithm based on analysis of the wandering trajectories [4, 7] would be applied to investigate stability of piezoelectric devices in control parameter planes/spaces. This methodology had been successfully applied both to smooth and non-smooth dynamical systems.

Acknowledgements

The work has been supported by the National Science Foundation of Poland under the grant MAESTR02 No. 2012/04/A/ST8/00738 for years 2012-2016.

References

1. Shen J., Jywe W., Chiang H., Shu J.: Precision Tracking Control of a piezoelectric-actuated system. *15th Mediterranean Conference on Control & Automation, Proceedings.* Athens, Greece, July 27-29, 2007, 6 pages.
2. Wood R., Steltz E., Fearing R.: Nonlinear performance limits for high energy density piezoelectric bending actuators, 8 pages.
3. Gutschmidt S.: *Mathematical-mechanical modeling of wobbling disk piezoelectric motors*. PhD thesis, Technical University of Darmstadt, P. Hagedorn, 2005, 99.
4. Awrejcewicz J., Dzyubak L.: Hysteresis modelling and chaos prediction in one- and two-dof hysteretic models. *Archive of Applied Mechanics*, 77, 2007, 261-279.
5. Agnes G.: *Performance of nonlinear mechanical, resonant-shunted piezoelectric and electronic vibration absorbers for multi-degree-of-freedom structures.* PhD thesis, Virginia Polytechnic Institute and state University, D. Inman, 1997, 151.
6. Ikeda T.: *Fundamentals of piezoelectricity*, Oxford University Press, Oxford, New York, Toronto, 1990.
7. Awrejcewicz J., Dzyubak L.: Chaos caused by hysteresis and saturation phenomenon in 2-dof vibrations of the rotor supported by the magneto-hydrodynamic bearing. *International Journal of Bifurcation and Chaos* 15(6), 2011, 2041-2055.

Jan Awrejcewicz, Professor: Technical University of Łódź, Department of Automatics and Biomechanics, 1/15 Stefanowskiego St., 90-924 Łódź, Poland (*awrejcew@p.lodz.pl*).

Larisa Dzyubak, Associate Professor: National Technical University "Kharkov Polytechnic Institute", Department of Applied Mathematics, 21 Frunze St., 61002 Kharkov, Ukraine, (*ldzyubak@kpi.kharkov.ua, dzyubak.larissa@interdiscipline.org*).